Attenuation of whistler waves through conversion to lower hybrid waves in the low-altitude ionosphere

X. Shao,[1] B. Eliasson,[1,2] A. S. Sharma,[1] G. Milikh,[1] and K. Papadopoulos[1]

[1]   VLF waves excited by powerful ground-based transmitters propagate in the Earth-ionosphere waveguide and leak through the ionosphere to the magnetosphere, where they are often recorded by satellites. Simulations of the propagation of whistler waves using coupled transionospheric VLF propagation and three-dimensional ray-tracing models have shown systematic overestimates of the VLF wavefield strength near 20 kHz in the magnetosphere by about 20 dB in the night and 10 dB during the day. The paper presents numerical simulations of the conversion between whistler and lower hybrid waves interactions in the presence of short-scale field-aligned density irregularities (striations) in Earth's lower ionosphere. The simulations, which incorporate a realistic ionospheric density profile, show that the mode conversion of whistler waves to lower hybrid waves leads to significant attenuation of whistler waves at altitudes between 90 and 150 km. The striation width plays an important role in the conversion efficiency between whistler and lower hybrid wave. Uniformly distributed striations with 8 m transverse size result in 15 dB attenuation in the 90–150 km propagation range, while a spectrum from 2 to 10 m results in 9 dB attenuation. It is argued that the attenuation of whistler waves in the presence of short-scale density striations in Earth's ionosphere can account for most of the observed ~20 dB loss in VLF intensity. Furthermore, it predicts that VLF/ELF waves with frequencies below 5 kHz will not suffer similar attenuation.

1.   Introduction

[2]   Injection of VLF waves generated by Navy transmitters or lightning discharges into the magnetosphere and the Radiation Belts (RB) are of extreme importance since they play an important role in the control of energetic electron fluxes trapped in the RB. The injected waves propagate in the whistler mode and their resonant interaction with trapped energetic electrons results in pitch angle scattering and enhanced particle precipitation. They are often considered responsible for the formation of the slot region between the inner and outer radiation belts [*Inan and Bell*, 1991; *Abel and Thorne*, 1998a, 1998b; *Inan et al.*, 2003; *Gemelos et al.*, 2009]. Recent observations [*Starks et al.*, 2008] from five different spacecraft indicate that the amplitude of the measured VLF signals in the 20 kHz range is lower by more than 20 dB at night and 10 dB during the day than used in the RB models. This has been termed as the "20 dB puzzle" and has been the subject of a number of recent studies [*Foust et al.*, 2010; *Ganguli et al.*, 2010; *Mishin et al.*, 2010; *Bell et al.*, 2008]. Recent DEMETER plasma wave observations above the NWC VLF transmitter at 19.8 kHz also indicate that the nominal 20 dB intensity decrease occurs at altitudes lower than 700 km.

[3]   *Starks et al.* [2008] used a model developed by *Helliwell* [1965] based on collisional attenuation along the whistler propagation path through the *D/E* region to account for the intensity loss. The 20 dB whistler power deficit reported by *Starks et al.* [2008] indicates the need for improved propagation models over those used by *Abel and Thorne* [1998a, 1998b] and *Bortnik et al.* [2003, 2006] to compute injection of VLF waves by ground transmitters and lightning. *Starks et al.* [2008] suggested that additional loss processes must be taken into account to model transionospheric propagation of whistler mode VLF radiation. *Lehtinen and Inan* [2009] performed full wave modeling of transionospheric propagation of VLF waves and the results are in agreement with analysis of *Starks et al.* [2008].

[4]   Recently, there have been several studies [*Foust et al.*, 2010; *Mishin et al.*, 2010] to identify the loss processes to account for the attenuation of whistler waves in the ionosphere. *Mishin et al.* [2010] studied the nonlinear VLF effects (parametric instabilities) driven by intense VLF pump waves in the topside ionosphere above powerful VLF transmitters such as the NWC VLF transmitter in Australia. They suggested that the nonlinear interactions may be responsible for part of the energy loss of VLF wave signals as they propagate through the heated ionosphere.

[1]Departments of Physics and Astronomy, University of Maryland, College Park, Maryland, USA.
[2]Institute for Theoretical Physics, Faculty of Physics and Astronomy, Ruhr-University Bochum, Bochum, Germany.

[5] *Bell et al.* [2008] applied the theory of mode coupling between whistler and LH waves in the presence of field-aligned plasma density irregularities [*Bell and Ngo*, 1990] to account for part of the whistler wave energy loss through linear mode conversion of whistler to so-called quasi-electrostatic whistler mode waves. Using the full set of equations, one can show that the electrostatic lower hybrid wave is on the same dispersion surface as the whistler wave. Therefore the oblique electrostatic waves can be referred to as quasi-electrostatic whistler mode waves [*Bell and Ngo*, 1990]. Hence, for the same frequency as the input transmitter signals, there are two possibilities, one with almost purely electromagnetic whistler wave propagating with a small angle to the magnetic field lines, and one almost electrostatic wave propagating across the magnetic field lines [*Stenzel and Gekelman*, 1975; *Vincena et al.*, 2008]. Adopting the notation of *Vincena et al.* [2008], we will refer to the electrostatic whistler waves as lower hybrid (LH) waves in this paper. In the past, the generation of LH waves by whistler waves and vice versa on density striations has been investigated theoretically for planar density irregularities [e.g., *Bell and Ngo*, 1990]. In experiments at Arecibo, it was also demonstrated that VLF signals can couple into ionospheric ducts and propagate into the conjugate hemisphere as ducted whistlers, where they can parametrically excite LH waves [*Lee and Kuo*, 1984]. In the 1990s, considerable attention was given to the observations of small-scale LH structures in the ionosphere. They were first interpreted as collapse of LH solitons which was later shown to be incorrect by *Schuck et al.* [2002]. Instead, these observations of what is now referred to as the Lower Hybrid Solitary Structures (LHSS) were found to be consistent with Whistler/LH/Whistler conversion owing to preexisting density structures in the ionosphere. A comprehensive review of the LHSS phenomenon is given by *Schuck et al.* [2003]. In laboratory experiments, *Rosenberg and Gekelman* [1998, 2000, 2001] studied the mode conversion of incident whistler waves into LH waves on a single striation at LAPD and found that the width of the striation plays an important role in determining the mode conversion efficiency.

[6] *Parrot et al.* [2007] observed the presence of ionospheric irregularities at altitude ∼700 km above NWC transmitter during VLF wave transmission. Motivated by this work, *Foust et al.* [2010] presented studies of the "20 dB deficit." To estimate the power loss of VLF whistler mode waves while propagating up to ∼700 km altitude at middle latitude, *Foust et al.* [2010] used a full wave model [*Bell and Ngo*, 1990; *Lehtinen and Inan*, 2008] and modeled whistler wave propagation assuming uniform background density corresponding to that at 700 km and a set of plausible field-aligned density irregularities. They found that for short propagation paths of ∼15 km, the model predicts power losses ranging from 3 dB (25% probability) to 7 dB (2% probability). For longer propagation paths of ∼150 km, the model predicts power losses ranging from 4 dB (25% probability) to over 10 dB (2% probability). The model of *Foust et al.* [2010] neglects processes occurring below the F peak and especially at altitudes between 100 and 200 km.

[7] It is the objective of the present paper to demonstrate that for plausible irregularity spectra the predominant power loss for whistler waves occurs at altitudes between 100 and 200 km. A full wave model of whistler wave propagation in the lower ionosphere is used to estimate the attenuation of whistler waves owing to mode conversion to LH waves in the presence of density striations and collisions. The simulations use a realistic night side nonuniform ionosphere density profile and address the "20 dB puzzle" for the whistler waves propagating through ionosphere.

[8] The paper is organized as follows. In section 2 we present a numerical model and simulation setup for modeling linear mode conversion between whistler wave and LH wave in the presence of short-scale density striations. We, furthermore, discuss the condition for resonant mode conversion between whistler and LH waves. In section 3 we discuss evidence, spectra and the physics of naturally driven striations between 100 and 200 km at middle latitude. In section 4 we use the numerical model to study the attenuation of whistler waves owing to mode conversion in the presence of density striations for different striation widths, and discuss their implications. Finally, the main conclusions are presented in section 5.

2. Interaction of Whistler Waves With Density Irregularities in the Inhomogeneous Low-Altitude Ionosphere

2.1. Simulation Model

[9] A 2D model is used to simulate the interaction of whistler waves with field-aligned density striations in an inhomogeneous plasma in the presence of collisions. The model is based on decomposition of the electron current density as $\vec{j}_e = \vec{j}_{LH} + \vec{j}_W$ and the wave electric field as $\vec{E} = \vec{E}_{LH} + \vec{E}_W$, where the subscripts LH and W denote "lower hybrid" and "whistler" waves, respectively, and leads to the equations [*Eliasson and Papadopoulos*, 2008]:

$$\frac{\partial \vec{j}_{LH}}{\partial t} = \nabla^{-2}\left\{\frac{e}{m_e}\nabla \times \left[\nabla \times \left(n_{str}\vec{E}_W + \vec{j}_{LH} \times \vec{B}_0\right)\right] \right. $$
$$\left. - \frac{e}{m_i}\nabla\left[\nabla \cdot \left(\vec{j}_{LH} \times \vec{B}_0\right)\right]\right\} - \nu_{in}\vec{j}_{LH} \qquad (1)$$

for the LH waves and to

$$\frac{\partial \vec{j}_W}{\partial t} = -\frac{e}{m_e}\left(1 - \lambda_e^2\nabla^2\right)^{-1}\nabla \times \left[\nabla \times \left(\lambda_e^2\left(n_{str}\vec{E}_{LH} + \vec{j}_W\right.\right.\right. $$
$$\left.\left.\left. \times \vec{B}_0 + \nu_{en}\vec{j}_W\right)\right)\right] \qquad (2)$$

for the whistler waves.

[10] Here, m_e and m_i are the electron and ion (typically oxygen ion) masses, n_{str} the striation density distribution, $\vec{B}_0$ the background magnetic field, and $\lambda_e = c/\omega_{pe}$, with the electron plasma frequency $\omega_{pe} = (n_0e^2/\varepsilon_0 m_e)^{1/2}$ for the background density n_0. In equation (1), the $n_{str}\vec{E}_W$ describes the coupling of the whistler electric field to the LH waves, and in equation (2), the $n_{str}\vec{E}_{LH}$ term describes the coupling of the LH electric field to whistler waves, in the presence of striations. For $n_{str} = 0$, equations (1) and (2) are decoupled, and describe the propagation of LH and whistler waves. Given the LH component of the electron current density $\vec{j}_{LH}$, the electrostatic field of the LH wave can be obtained as [*Eliasson and Papadopoulos*, 2008]

$$\vec{E}_{LH} = \frac{1}{n_0}\nabla\nabla^{-2}\left[\nabla \cdot \left(\vec{j}_{LH} \times \vec{B}_0\right)\right], \qquad (3)$$
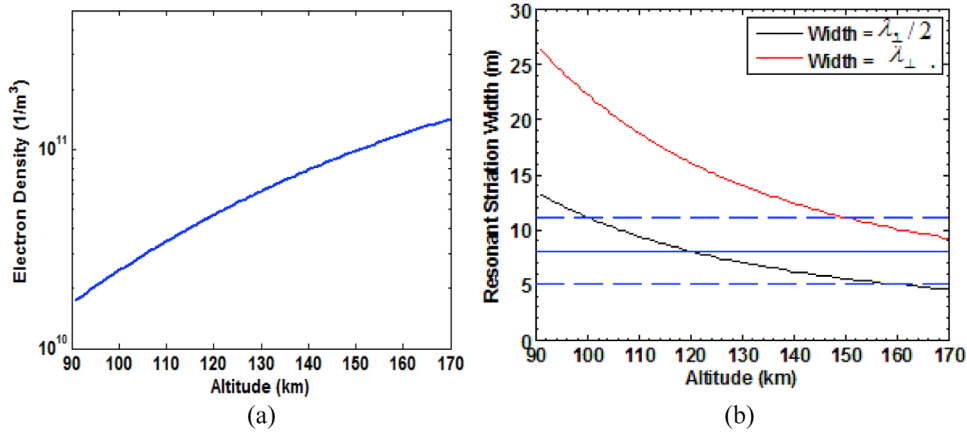
Figure 1. (a) Electron number density profile versus altitude used in the simulations. (b) Density striation width D_{str} versus altitude for resonant whistler and LH conversion for frequency $f = 18$ kHz in ionosphere as prescribed in Figure 1a for striation width satisfying $D_{str} = \frac{\lambda_\perp}{2}$ and $D_{str} = \lambda_\perp$.

while the whistler wave electric field as

$$\vec{E}_W = -\frac{1}{n_0}\vec{j}_W \times \vec{B}_0. \tag{4}$$

Equations (1)–(4) form the set of equations for modeling the propagation of coupled whistler and LH waves in the presence of density striations. Equations (1) and (2) are slightly modified from *Eliasson and Papadopoulos* [2008, equations (22) and (23)] by taking into account the inhomogeneous background electron density profile along the z direction and the effects of ion-neutral and electron-neutral collisions, with frequencies ν_{in} and ν_{en}, respectively.

2.2. Resonant Mode Conversion

[11] The mode conversion of whistler waves into LH waves occurs most efficiently when the parallel component of the wave vectors of the whistler and the LH wave for the same frequency are equal. For a collisionless homogeneous plasma, this condition can be obtained by using the dispersion relations of a parallel propagating whistler:

$$\omega = \frac{c^2 k_z^2}{\omega_{pe}^2}\omega_{ce}, \tag{5}$$

and a LH wave in the electrostatic limit ($\lambda_e^2 k^2 \gg 1$):

$$\omega^2 = \frac{\omega_{ce}\omega_{ci}k_\perp^2 + \omega_{ce}^2 k_z^2}{k_\perp^2 + k_z^2}, \tag{6}$$

where ω_{ce} and ω_{ci} are the electron and ion gyrofrequencies, respectively. The resonant mode conversion condition for LH to whistler waves can be obtained by combining equations (5) and (6). By solving these equations for the value of $k_\perp$, we find that

$$k_\perp^2 = \frac{\omega_{ce}^2 - \omega^2}{\omega^2 - \omega_{ce}\omega_{ci}}\frac{\omega}{\omega_{ce}}\frac{\omega_{pe}^2}{c^2}. \tag{7}$$

Equation (7) is the resonance condition and implies that the wave frequency ω needs to satisfy $\sqrt{\omega_{ce}\omega_{ci}} < \omega < \omega_{ce}$ for the LH wave to resonate with the whistler wave.

[12] The assumption of parallel whistler propagation along the magnetic field lines is not always true. For example, the anomalous attenuation exists above VLF transmitters located near the magnetic equator (NPM), as well as above VLF transmitters located at much higher latitudes (NAA). Over NPM, Earth's magnetic field has a dip angle of about 50 degrees, while over NAA this dip angle is about 75 degrees. To treat the case of oblique magnetic field, the factor k_z^2 in equation (5) should be replaced by kk_z, where $k = \sqrt{k_\perp^2 + k_z^2}$ is the modulus of the wave vector of the vertically propagating whistler wave. Equation (5) combined with equation (6) then gives the more general resonance condition, which, however, is more complicated. For simplicity, we assume parallel propagation of the whistler waves below.

[13] For whistler waves propagating along a density striation of transverse width D_{str}, the resonant condition occurs when the transverse component of the LH wave forms a standing wave inside the striation:

$$D_{str} = \frac{n}{2}\lambda_\perp, \tag{8}$$

where $\lambda_\perp = 2\pi/k_\perp$ is the transverse LH wavelength and n is a positive integer. Equation (8) is the condition for optimal resonant mode conversion between whistler and LH waves. Such a condition was derived previously by *Bell and Ngo* [1990] for whistler to LH conversion and found numerically by *Eliasson and Papadopoulos* [2008] for LH to whistler conversion.

[14] For a nonuniform ionospheric density profile the LH-whistler resonant mode conversion condition (equation (8)) requires that the striation width varies with altitude as is illustrated in Figure 1. Figure 1a shows the altitude dependence of the electron number density $n_0(z)$ used in our simulations. It is chosen to be close to the profile of a typical nighttime ionosphere. Figure 1b shows the altitude dependence of the resonant density striation width as calculated from equations (7) and (8) for wave frequency $f = 18$ kHz. The density striations usually have gradual transverse profiles and it is expected that the LH-whistler resonant mode

conversion condition, equation (8), can be satisfied over a range of altitudes. In Figure 1b, we choose a range of density striation widths $D_{str} = 8 \pm 3$ m and mark them with three horizontal blue lines. It can be seen that in this case, the interaction region can cover an altitude range from 100 km to 160 km.

3. Field-Aligned Density Irregularity Spectra

[15] Similarly to *Foust et al.* [2010] an important ingredient of our theory is the presence of naturally occurring density irregularity spectra. However, our focus is in the low-altitude, inhomogeneous ionosphere between 100 and 180 km in the presence of collisions. Density striations such as hypothesized here have been observed in the ionosphere under a variety of conditions. Simultaneous rocket and radar observations in the midlatitude *E* region have measured strong field-aligned density depletions at altitudes 80–150 km with meter-like transverse scale size [*Fukao et al.*, 1998; *Tsunoda et al.*, 1998; *Yamamoto et al.*, 1998]. The irregularities are often associated with large-scale structures such as sporadic *E* or the so-called quasi-periodic (Q-P) structures. The sporadic *E* layers are either steady or variable, with the latter occurring significantly more often, and with higher occurrence probability at night. Incoherent scatter observations of plasma density profiles at midlatitude show large-scale waves with both type 1 and 2 characteristics. The Q-P structures are tilted vertical striations at altitudes near 110 km during postsunset period [*Yamamoto et al.*, 1991; *Kelley et al.*, 1995]. Their radar echoes show horizontal scales of 15–30 km and lead to the meter-scale density irregularities or striations by mechanisms similar to those of type 1 and 2 irregularities in the equatorial ionosphere [*Sudan*, 1983]. The large-scale electric fields or density gradients lead to drifts which drive two-stream and gradient drift instabilities. The instabilities have different spectral characteristics depending on the strength of the drift [*Schlegel and Haldoupis*, 1994] and the threshold for the drift speed is modified, compared to the equatorial case, owing to the heavy metal ions at middle latitudes. When the drift is above threshold, namely higher than the ion sound speed, a narrow spectrum of irregularities is generated by the Farley-Buneman instability. For lower drift speeds a broad type 2 turbulence is generated, resulting in a cascade of irregularities with scales from the kilometer scale down to the meter scale [*Pfaff et al.*, 1998]. The radar echoes of the irregularities show 6.1 m for 24.5 MHz, with strong spectral broadening [*Tsunoda et al.*, 1998] and 3.2 m for 46.5 MHz [*Yamamoto et al.*, 1991]. The field-aligned irregularities thus range from a few to tens of meters.

[16] Another mechanism for the generation of field-aligned irregularities is the thermal instability driven by the neutral wind [*Kagan and Kelley*, 2000]. The neutral wind induces polarization electric fields, which in turn produces Ohmic heating. In the density depleted regions this leads to enhanced plasma pressure and consequently the plasma is forced out, thus increasing the density depletion. This thermal instability mechanism predicts the scale sizes of the density depletions along the magnetic field to be more than two orders of magnitude compared to the transverse sizes. These two mechanisms for producing field-aligned irregularities, or striations, yield transverse scale sizes ranging from a few to tens of meters in the midlatitude *E* region.

4. Simulation Results

4.1. Simulation Setup

[17] We solve equations (1)–(4) numerically to study the attenuation of whistler waves owing to the conversion to LH waves along the propagation path in a nonuniform ionosphere. The simulation domain is chosen to be a rectangular box with typical box size $L_y \times L_z = 120$ m $\times$ 90 km and the number of grid points $N_y \times N_z = 300 \times 1350$, resulting in grid sizes of $\Delta y = L_y/N_y = 0.4$ m, and $\Delta z = L_z/N_z = 66.7$ m. The large aspect ratio between the *z* and *y* directions for the grid sizes and the simulation box is required owing to the propagation characteristics of the LH waves with $k_\perp$ being much larger than k_z. The spatial derivatives are approximated with a pseudospectral method with periodic boundary conditions used in both the *y* and *z* directions. A fourth-order Runge-Kutta scheme is used to advance the solution in time, and the simulation time step is chosen to be $\Delta t = 3 \times 10^{-8}$ s. The simulation is computationally intensive and typically takes one week to finish on a two-core high-end workstation.

[18] Our numerical parameters have been chosen to resolve the problem accurately. The fourth-order Runge-Kutta method is accurate as long as the time step is much smaller than the wave period. With a wave frequency of 18 kHz, the wave period is 5.6×10^{-5} s. The chosen time step $\Delta t = 3 \times 10^{-8}$ s is 1800 times shorter than the wave period, and hence the numerical errors due to the time stepping are negligible. The relatively short time step is chosen owing to the stability condition for the Runge-Kutta method, $\Delta t < \sqrt{8}/f_m$, where f_m is the largest eigenvalue of the problem. For our problem, f_m is approximately equal to $\Omega_{ce} = 8.44 \times 10^6$ s^{-1}, which requires that the time step $\Delta t < 3.35 \times 10^{-7}$ s. The chosen time step $\Delta t = 3 \times 10^{-8}$ s satisfies this condition.

[19] The pseudospectral method is used to calculate the spatial derivatives. It is based on (1) the interpolation of the grid function by a trigonometric polynomial (series), (2) the exact differentiation of the trigonometric polynomial, and (3) the evaluation of the result on the numerical grid. In practice the grid function is first Fourier transformed in space (using the fast Fourier transform), then multiplied by the wave number (or a combination of wave numbers), and the inverse Fourier transformed to obtain the result. The result is exact if the solution can be represented on the numerical grid, and the pseudospectral method does not introduce any numerical dispersion errors, in contrast to finite difference methods. The restriction is set by the Nyqvist theorem, which states that more than two grid points per wavelength are needed to represent a solution on the numerical grid. Hence the largest wave numbers allowed (the Nyqvist wave numbers) in the simulation are given by $k_\perp < {}^\pi/_{\Delta y}$ and $|k_z| < {}^\pi/_{\Delta z}$. We have $\Delta y = 0.4$ m and $\Delta z = 66.67$ m, which gives the Nyqvist wave numbers ${}^\pi/_{\Delta y} = 7.9$ m^{-1} and ${}^\pi/_{\Delta z} = 4.7 \times 10^{-2}$ m^{-1}, where Δy and Δz are the grid sizes in the *y* and *z* directions. The perpendicular and parallel wave numbers at the upper boundary of the
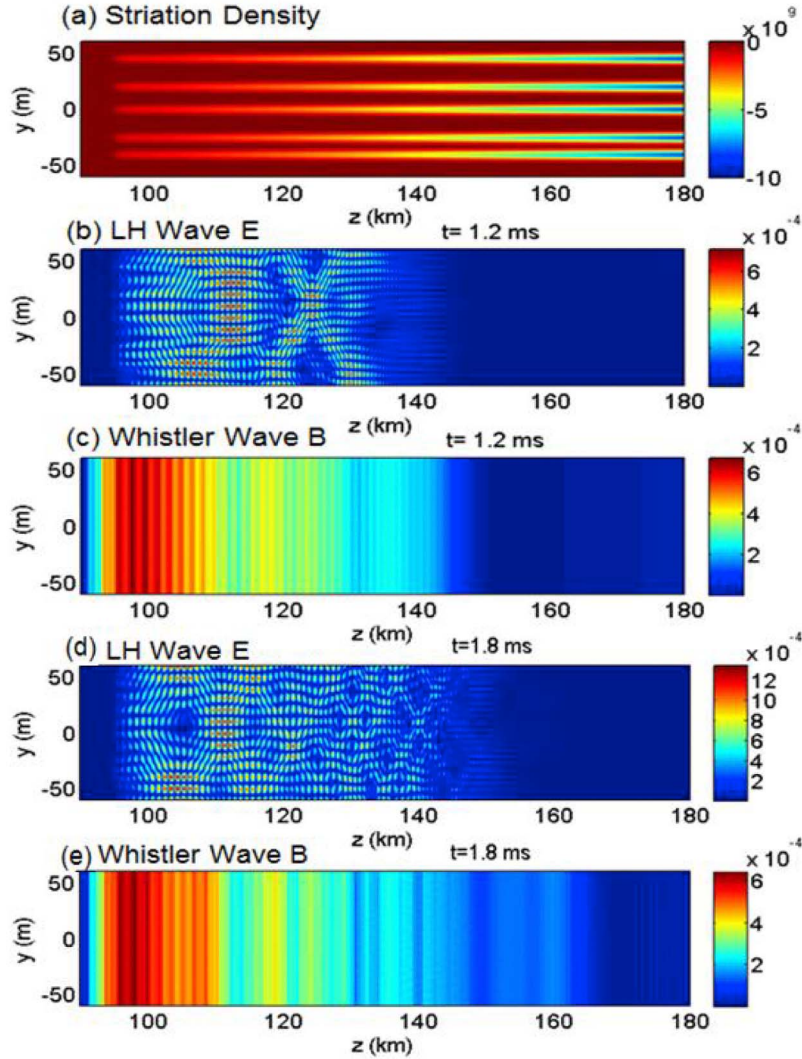
Figure 2. Attenuation of whistler waves through mode conversion to LH waves in the presence of density striations. (a) Distribution of density striations with Gaussian profile and width $D_{str} = 8$ m and amplitude 5% of the background density. Their centers are located at $y_{sc} = -40$ m, -25 m, 0 m, 20 m, 45 m. (b and d) Distribution of LH wave electric field amplitude at $t = 1.2$ ms and 1.8 ms. (c and e) Distribution of the whistler wave magnetic field amplitude.

simulation domain, where the wave number is largest (owing to the largest density; see Figure 1a) are obtained from (5) and (7) as $k_\perp = 0.68$ m^{-1} and $k_z = 0.8 \times 10^{-2}$ m^{-1}, which are much smaller than the corresponding Nyqvist wave numbers.

[20] Hence, both the whistler and lower hybrid waves are well represented on the numerical grid. The striations are also resolved with at least 5–10 grid points, which gives high enough resolution.

[21] In the simulation setup, the external magnetic field $\vec{B}_0 = B_0\hat{z}$, with $B_0 = 4.8 \times 10^{-5}$ T, is aligned with the z axis. The corresponding electron and ion (oxygen) gyrofrequencies are $\omega_{ce} = 8.44 \times 10^6 s^{-1}$ and $\omega_{ci} = 286.1 s^{-1}$, respectively. The simulation domain spans from $z = 90$ to 180 km in altitude with a nonuniform background density, as shown in Figure 1a. The density striations are also aligned along the z direction with a Gaussian profile in the transverse y direction:

$$n_{str}(z) = -n_{0,str}(z) \exp\left(-\frac{(y - y_{sc})^2}{\Delta_{str}^2}\right), \qquad (9)$$

with $D_{str} = 2\Delta_{str}$. For the simulations presented here, we use $n_{0,str}(z) = 0.05 n_0(z)$ (5% of the background number density) and place 5 density striations centered at $y_{sc} = -40$ m, -25 m, 0 m, 20 m, and 45 m. The striation width D_{str} is varied in different simulations and the case of $D_{str} = 8$ m is shown in Figure 2a.

[22] To simulate the continuous injection of whistler waves, we use an external current source

$$\vec{j}_{ws} = j_{w0} \tanh^2(t/D_t) \sin(k_0 z - \omega t)/\cosh[(z - z_0 - dz)/dz]\hat{y}, \qquad (10)$$

where $j_{w0} = 8.8 \times 10^9$ A/m^3, the risetime $D_t = 0.1$ ms, $\omega = 2\pi f$ with the injection wave frequency $f = 18$ kHz, $k_0 = 0.003$ m^{-1}, $z_0 = 90$ km and $dz = 2$ km, and the waves propagate upward from the bottomside ionosphere. The use of the reciprocal of the "cosh" function in equation (10) ensures that the current source is located in a region between $z = 90$ and 95 km.

4.2. Simulation With Striation With Width $D_{str} = 8$ m

[23] The first set of simulations were performed to study the propagation of a whistler wave and its interactions with a collection of density striations with Gaussian profiles as specified in equation (9) and all striations having the same width $D_{str} = 8$ m. Figures 2b, 2c, 2d, and 2e show the spatial distribution of the LH wave electric field and the whistler wave magnetic field amplitudes at $t = 1.2$ ms and 1.8 ms. Note that the simulation domain spans from $z = 90$ km to 180 km in Figure 2. In order to assess the effects on whistler wave attenuation owing to the mode conversion to LH waves in the presence of density striations, we set the collisional frequencies $\nu_{in} = \nu_{en} = 0$ in the simulation. Since the whistler waves are injected continuously from the bottom of the ionosphere, the snapshots of the wavefield amplitude distributions provide an overview of the attenuation of the whistler waves and their conversion to LH waves along the propagation path. Figures 2b and 2d show that during the interaction between the whistler wave and the striations. The excited LH waves propagate along the magnetic field lines in the z direction and have short-scale structures in the y direction. While the LH wave vector is almost perpendicular to the magnetic field, its group velocity is perpendicular to the wave vector and thus almost parallel to the magnetic field. Figures 2c and 2e show the attenuation of the whistler waves owing to the conversion to LH waves. At $t = 1.2$ and 1.8 ms the whistler wavefront has traveled a distance of ~50 and 70 km along z, respectively. Notice that the whistler wave slows down owing to the increase in the density and the associated decrease of the group velocity along its path.

[24] In order to quantitatively assess the attenuation of the whistler wave owing to mode conversion to LH waves, we integrate the whistler wave magnetic energy over y and obtain [*Eliasson and Papadopoulos*, 2008]

$$W_B(z) = \int_{-L_y/2}^{L_y/2} \frac{B^2}{2\mu_0} dydz \approx \int_{-L_y/2}^{L_y/2} \frac{m_e}{2\lambda_e^2 n_0(z)} \left(\nabla^{-2}\nabla \times \vec{j_e}\right)^2 dy \frac{L_z}{N_z} \tag{11}$$

and LH wave energy

$$W_{LH}(z) = W_e(z) + W_i(z), \tag{12}$$

where

$$W_e(z) = n_0(z) \int_{-L_y/2}^{L_y/2} \frac{m_e v_e^2}{2} dydz = \frac{m_e}{2n_0(z)} \int_{-L_y/2}^{L_y/2} j_e^2 dy \frac{L_z}{N_z} \tag{13}$$

and

$$W_i(z) = n_0(z) \int_{-L_y/2}^{L_y/2} \frac{m_i v_i^2}{2} dydz \approx \frac{m_i}{2n_0} \int_{-L_y/2}^{L_y/2} \left[\nabla^{-2}\nabla\left(\nabla \cdot \vec{j_e}\right)\right]^2 dy \frac{L_z}{N_z} \tag{14}$$

are the electron and ion kinetic energies, respectively.

[25] Figure 3 (top, middle) shows the calculated z distribution of whistler wave and LH wave energy integrated over y. To serve as a reference, Figure 3 (top) also shows the simulated spatial distribution of whistler wave energy over z if it propagates without conversion to LH waves and other losses. This result is obtained by setting $n_{str}(y, z) = 0$ and $\nu_{in} = \nu_{en} = 0$ in equations (1)–(4). The increase of the whistler wave amplitude along z is due to the decrease of the whistler wave group speed as it propagates into the ionosphere with increasing electron density. We can see from Figure 3 (top) that the whistler waves are attenuated significantly for the simulation with density striations as compared to that without striations. Figure 3 (middle) indicates that the attenuation of the whistler waves is accompanied by the increase of the LH wave energy owing to whistler-LH wave mode conversion. The LH wave energy with large oscillatory pattern concentrates mainly between $z = 100$ and 150 km. We define the whistler wave attenuation factor as

$$A_w = -10 \log_{10}\left(W_{B,str}(z)/W_{B,0}(z)\right) \ \ (\text{dB}), \tag{15}$$

where $W_{B,str}(z)$ and $W_{B,0}(z)$ are the whistler wave energies with and without the density striations, respectively. Figure 3 (bottom) shows the whistler wave attenuation factor versus z and it clearly shows an increase along the propagation path of the whistler waves. For the whistler wave propagating from 90 km to 150 km, the attenuation factor is ~15.5 dB from the simulation with 5 density striations of width $D_{str} = 8$ m. The most significant attenuation of whistler waves occurs between $z = 100$ km and 150 km, which is consistent with the resonant mode condition for striations in a nonuniform ionosphere, as presented in Figure 1b. In Figure 1b, the altitude range for resonant mode conversion is from $z = 100$ to 140 km for striations with fixed width $D_{str} = 8 \pm 3$ m. For striations with a Gaussian shape with width $D_{str} = 8$ m, the striation boundary changes gradually and therefore the mode conversion interaction region can cover a region from $z = 100$ to 150 km.

[26] It is expected that including the effect of ion-neutral collisions will damp the LH wave, as is evident from equation (2). However, it is not clear how much this will affect the attenuation of whistler wave indirectly, since the LH waves can mode convert back to the whistler waves through interaction with the striations [*Eliasson and Papadopoulos*, 2008]. In order to examine this, another set of simulations was carried out by including the ion-neutral collisions and the results are shown in Figure 4b. The simulation of mode conversion in the presence of collisions show much less energy in the LH waves, compared to the case with no collisions (Figure 4b, bottom). This is due to damping of the LH waves by ion-neutral collisions, as shown in equation (1). However, there is not much difference in the whistler wave energy distribution versus z for the simulations with or without collisions (black and red curves in Figure 4b, top).

4.3. Effects of Density Striation Widths on Whistler Wave Attenuation

[27] To investigate the effects of the striation width on the whistler wave attenuation owing to mode conversion to LH waves, we simulate whistler wave propagation using the same background ionosphere as above, but with different
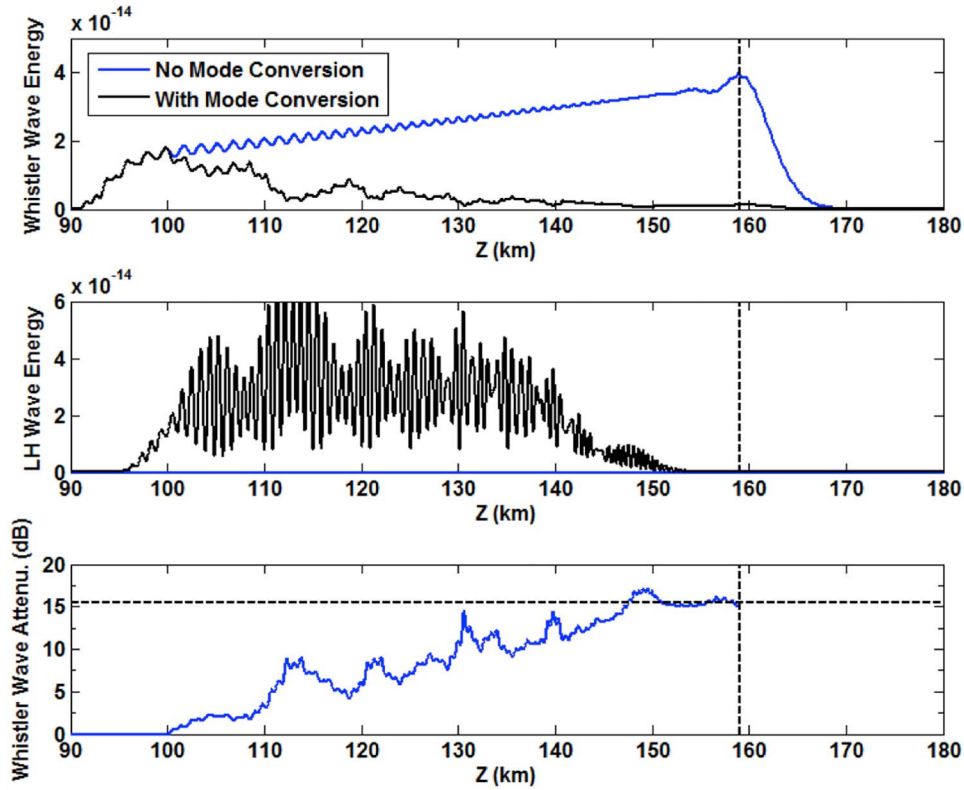
Figure 3. (top) Spatial variation of y-integrated whistler wave energy along z obtained from simulation with and without whistler-LH wave mode conversion (black and blue curve, respectively) at time $t = 1.8$ ms. (middle) Corresponding to the LH wave (black curve). (bottom) Attenuation factor (in decibels) for the whistler wave along the propagation path. All panels are derived from Figure 2b at $t = 1.8$ ms.

striation widths. Figures 5 and 6 show simulation results with uniformly distributed density striations of Gaussian shape with widths $D_{str} = 2$ m and 15 m, respectively. The attenuation factors at $z = 140$ km obtained from the simulation with $D_{str} = 2$ m and 15 m are ∼2.2 dB and 4 dB, respectively. This is consistent with our analysis of resonant mode conversion condition (8) for whistler and LH waves in the presence of density striations. In Figure 1b, one can see that for striation with fixed width $D_{str} = 2$ m, there is no resonant mode conversion between the altitudes $z = 90$ km and 170 km. Therefore, the attenuation of whistler wave owing to mode conversion to LH wave is not significant for striation of Gaussian width $D_{str} = 2$ m. As for striations with Gaussian width $D_{str} = 15$ m (Figure 6), the resonant mode conversion occurs mainly around $z = 100$ to 120 km, which is mainly due to the conversion of whistler wave to LH wave with transverse wavelength satisfying the condition of $\lambda_\perp = D_{str}$ (see Figure 1b).

[28] The above simulations clearly show that the striation width plays an important role in the attenuation of the whistler waves through mode conversion to LH waves. The radar and rocket observations of striations, discussed in section 3, show a spectrum of striation widths and simulations of such a case is shown in Figure 7. For mixed density striations with widths ranging from 2 m to 10 m, the overall attenuation factor at $z = 140$ km is ∼8.8 dB.

4.4. Comparison of Attenuation Factors

[29] The whistler wave attenuation factors owing to mode conversion to LH waves in the presence of various density striation widths are shown together in Figure 8. Also shown in Figure 8 is the attenuation owing to the electron neutral collision only (blue curve), calculated from the whistler wavefield propagation model [*Helliwell*, 1965]:

$$B_{1(z)} = B_1(z_s) \frac{\omega_{pe}(z)}{\omega_{pe}(z_s)} \exp\left[-\int_{z_s}^z \frac{\omega^{1/2}\omega_{pe}(z')\nu_{en}(z')}{2c\omega_{ce}^{3/2}} dz'\right]. \quad (16)$$

By defining $\alpha(z) = \exp\left[-\int_{z_s}^z \frac{\omega^{1/2}\omega_{pe}(z')\nu_{en}(z')}{2c\omega_{ce}^{3/2}} dz'\right]$, the attenuation factor owing to electron-neutral collisions is calculated as

$$A_w(z) = -20 \log_{10}(\alpha(z)). \quad (17)$$

We use the altitude-dependent electron-neutral collision frequency shown in Figure 4a to obtain the attenuation factor owing to the electron-neutral collision alone.

[30] From Figure 8, we see that the attenuation factor owing to the electron-neutral collision is ∼2 dB and the main attenuation occurs between $z = 80$ and 100 km. The attenuation factor is ∼12 dB at $z = 140$ km for whistler wave propagation in the presence of uniformly distributed density striations with Gaussian width = 8 m, which is the largest in
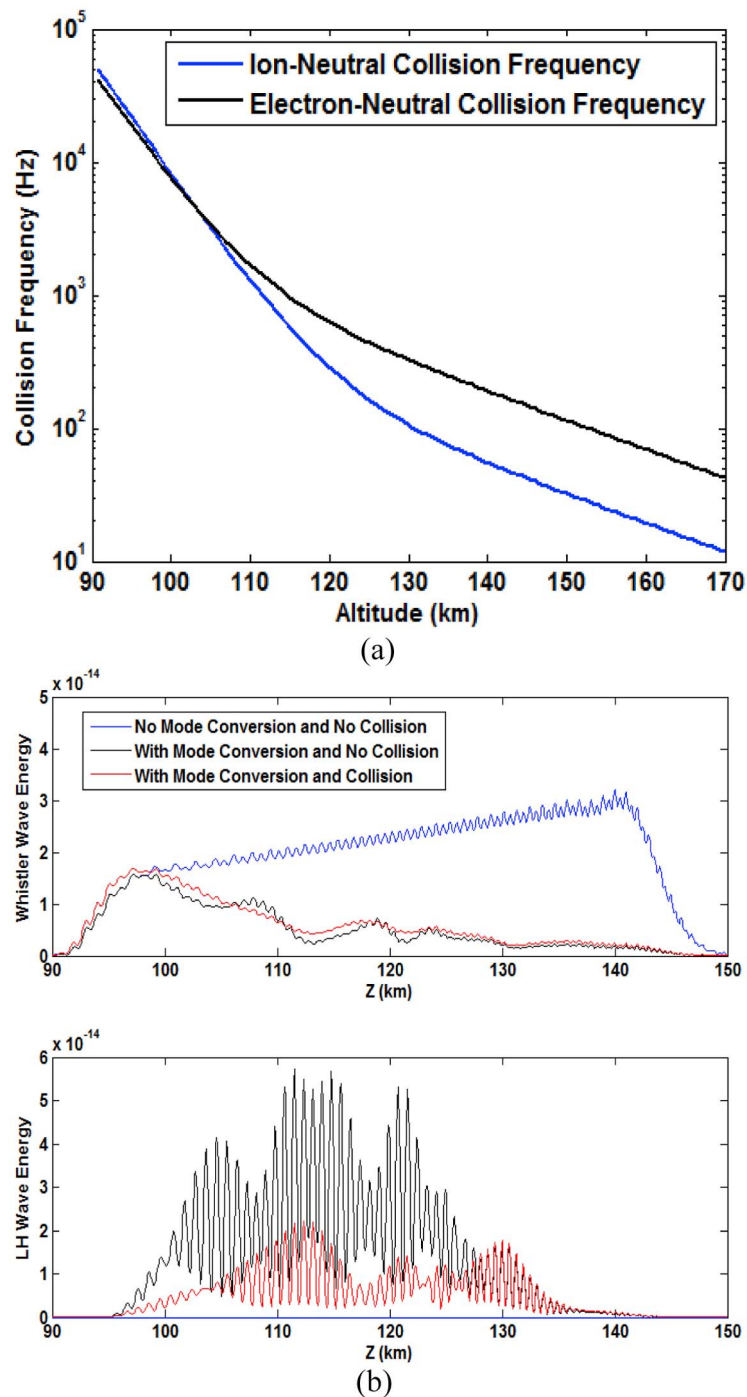
Figure 4. (a) Model of altitude-dependent ion-neutral collision frequency (blue curve) used in our simulations. The altitude-dependent electron-neutral collision frequency is also plotted and later used in section 4.5 to derive the whistler wave attenuation factor owing to only electron-neutral collisions. (b) Comparison of whistler (top) and lower hybrid (bottom) wave energies without mode conversion and ion-neutral collisions (blue curve), with mode conversion and no collisions (black curve), and with both mode conversion and collisions (red curves) at $t = 1.2$ ms.

comparison with the cases of other striation widths. This is consistent with resonant mode conversion as presented in Figure 1b, which shows that the condition is satisfied for fixed striation width = 8 ± 3 m between $z = 100$ and 140 km

in the nonuniform ionosphere used in the simulation. With density striations of mixed widths, the attenuation factor is about 9 dB. Thus, the attenuation owing to the mode
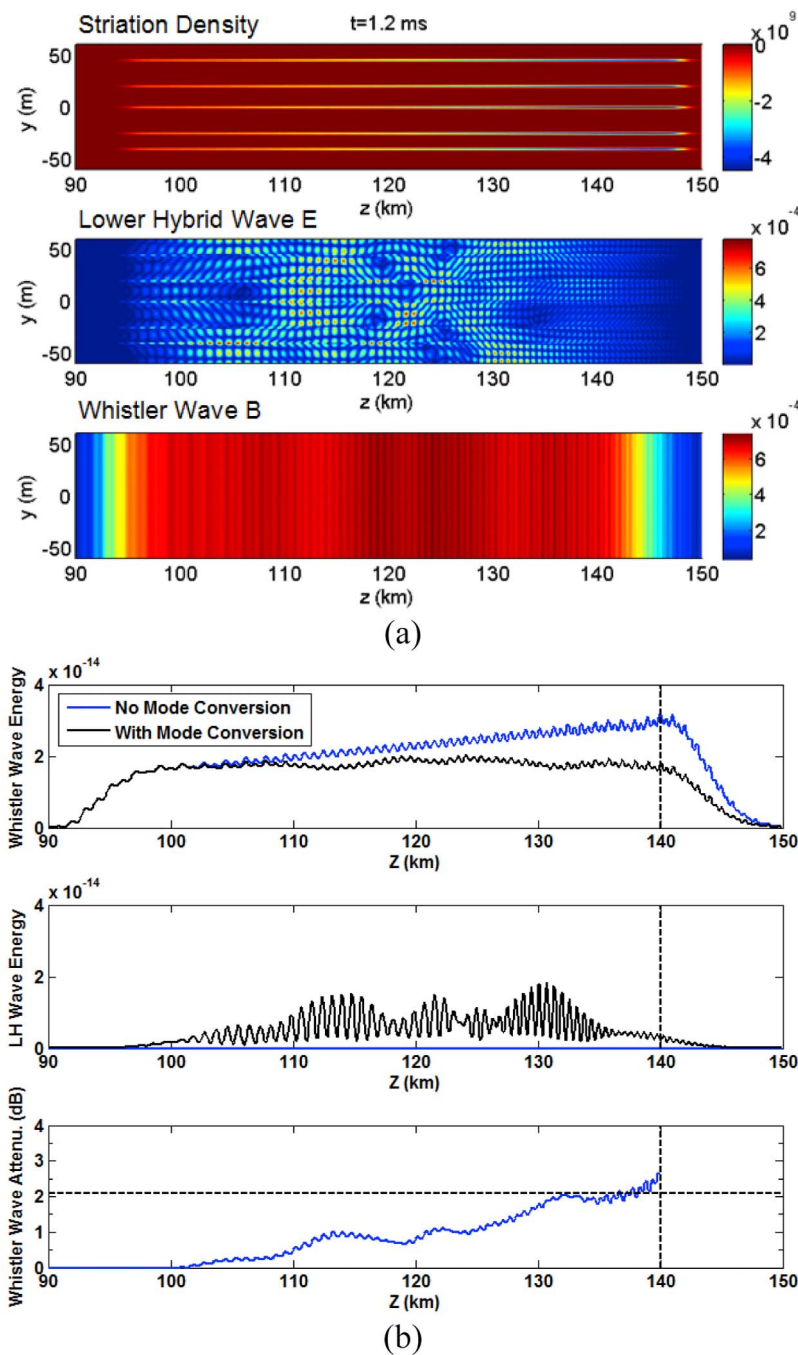
Figure 5. Conversion of whistler to lower hybrid waves in the presence of striations with width D_{str} = 2 m, and 5% amplitude of local density, at t = 1.2 ms. (a) From top to bottom: distribution of density striations with their centers located at the same y locations as in Figure 2, distribution of LH wave electric field amplitude, and distribution of whistler wave magnetic field amplitude. (b) From top to bottom: spatial variation of y-integrated whistler wave energy along z obtained from simulation without and with whistler-LH wave mode conversion (blue and black curve), spatial distribution of y-integrated LH wave energy along z for simulation with whistler-LH wave mode conversion (black curve), and attenuation factor in decibels for the whistler waves along the propagation path.
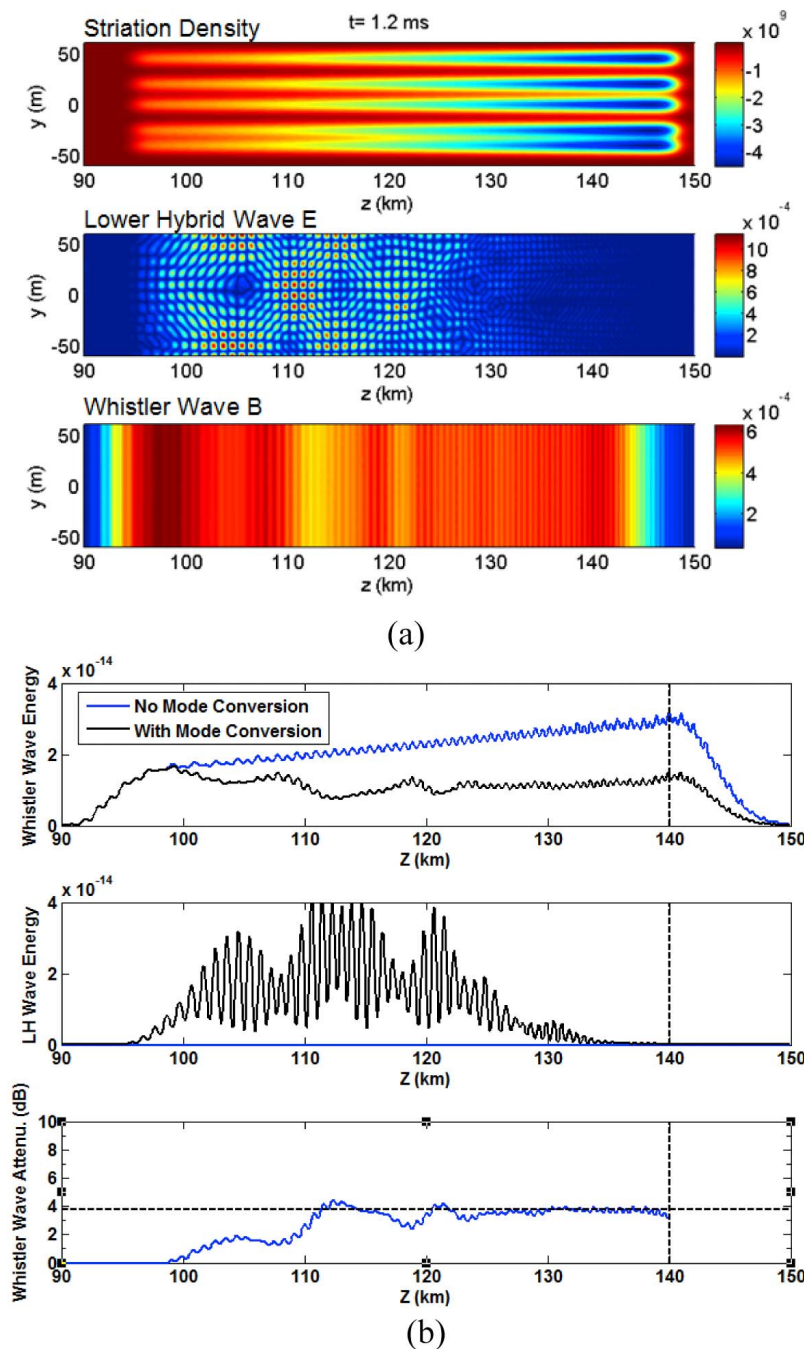
(a)

(b)

Figure 6. Similar plots as in Figure 5. The simulation is conducted in an ionosphere with density striations with the width $D_{str} = 15$ m.

conversion of whistler waves to LH waves is much stronger than that owing to the electron-neutral collisions.

5. Discussion

[31] We have developed a numerical model to simulate the mode conversion of whistler waves into LH waves in the presence of density striations in the nonuniform lower ionosphere. The simulations show that the striations lead to whistler wave attenuation by mode conversion to LH waves, and their widths play an important role in the attenuation rate. The LH waves are excited most effectively for striations with widths matching the condition of resonant mode conversion. Furthermore, the whistler wave attenuation is most significant when the product of the striation width and the wave number of the LH wave are of the order unity. The simulations show that for striations with fixed width of 8 m, the whistler wave attenuation can be as high as 15 dB for the ionospheric density profile used. With mixed density striations of widths ranging from 2 to 10 m, the whistler wave can be attenuated by ~9 dB as it propagates from 90 to 150 km. Therefore, for the density striation models
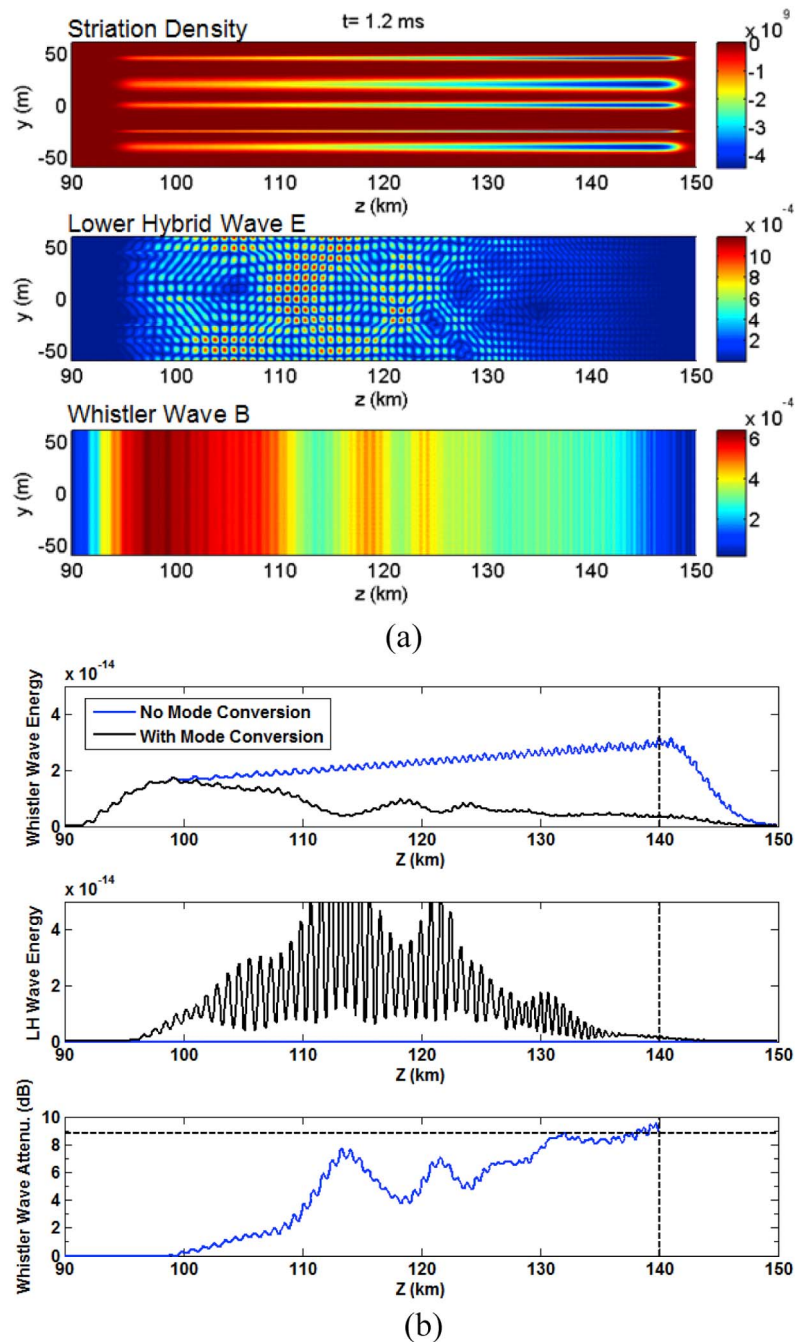
(a)

(b)

Figure 7. Similar plots as in Figure 5. The simulation is conducted in an ionosphere with density striation of mixed striation widths. The Gaussian striation widths are D_{str} = 8 m, 2 m, 6 m, 10 m, and 4 m at y_{sc} = −40 m, −25 m, 0 m, 20 m, and 45 m, respectively.

investigated, the mode conversion of whistler wave to LH waves can result in significant attenuation of VLF whistler waves as they propagate through the low-altitude ionosphere. Although the field-aligned plasma density irregularities or striations used in the simulations are consistent with the rocket and radar observations [*Yamamoto et al.*, 1991, 1998; *Kelley et al.*, 1995; *Pfaff et al.*, 1998], it is worth of pointing out that like any natural phenomenon, the striation widths are not always as perfect as would be necessary for an efficient conversion as the calculations given in this article indicate. However, the loss of whistler power is

also not always 20 dB. It is possible that this lack of perfect grating width in nature all the time may explain the intermittency or irregularity in the magnitude of power loss. A comparison of more detailed observations of striation characteristics and their correlation with the whistler power loss would be very useful as a future extension of this work.

[32] Whistler waves are important in the pitch angle scattering and precipitation of energetic electrons in Earth's radiation belts, and it is necessary to develop a whistler wave propagation model incorporating a comprehensive set of loss processes. The 20 dB whistler wave power deficit reported
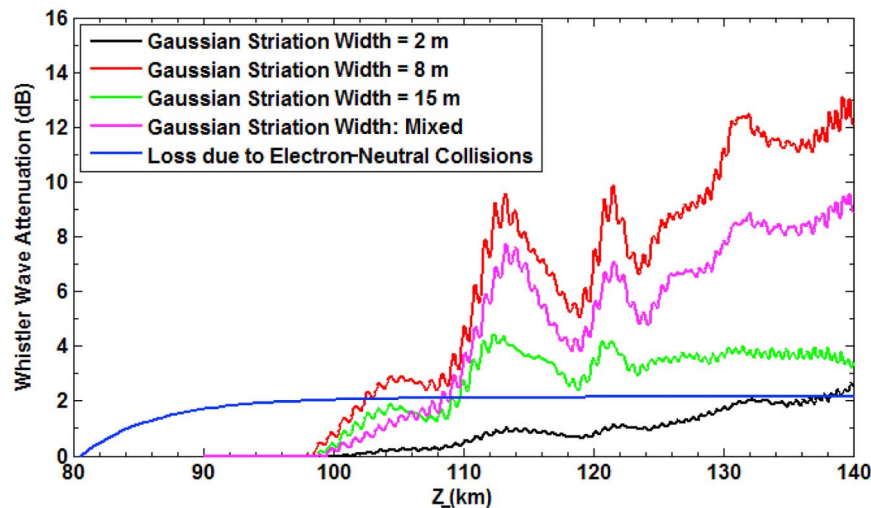
Figure 8. Comparison of the whistler wave attenuation factor versus altitude *z* from the simulations of whistler-LH wave mode conversion with density striations of different widths as well as owing to electron-neutral collisions alone.

by *Starks et al.* [2008] calls for such modeling efforts. The study by *Foust et al.* [2010] show that the mode conversion of whistler wave to LH waves in the middle altitude can result in 7–10 dB power loss for whistler waves. Our simulations show that the mode conversion in the low-altitude ionosphere can result in ∼10 dB power loss for whistler waves. A comprehensive modeling work to address the 20 dB whistler wave power deficit needs to take into account of mode conversion of whistler wave to LH waves in both lower and middle altitudes. On a speculative basis, we can consider the satisfaction of the resonance condition equation (7) combined with the fact that naturally driven irregularities have scale lengths in the range of 0–20 m, we can conclude that frequencies below 3–5 kHz will suffer very little attenuation in traversing the ionosphere. Whether other processes such as parametric instabilities or whistler turbulence [*Mishin et al.*, 2010; *Ganguli et al.*, 2010] will affect those lower frequencies is currently under study.

References

Abel, B., and R. M. Thorne (1998a), Electron scattering loss in Earth's inner magnetosphere: 1. Dominant physical processes, *J. Geophys. Res.*, *103*, 2385–2396, doi:10.1029/97JA02919.

Abel, B., and R. M. Thorne (1998b), Electron scattering loss in Earth's inner magnetosphere: 2. Sensitivity to model parameters, *J. Geophys. Res.*, *103*, 2397–2407, doi:10.1029/97JA02920.

Bell, T. F., and H. D. Ngo (1990), Electrostatic lower hybrid waves excited by electromagnetic whistler mode waves scattering from planar magnetic field-aligned plasma density irregularities, *J. Geophys. Res.*, *95*, 149–172, doi:10.1029/JA095iA01p00149.

Bell, T. F., U. S. Inan, D. Piddyachiy, P. Kulkarni, and M. Parrot (2008), Effects of plasma density irregularities on the pitch angle scattering of radiation belt electrons by signals from ground based VLF transmitters, *Geophys. Res. Lett.*, *35*, L19103, doi:10.1029/2008GL034834.

Bortnik, J., U. S. Inan, and T. F. Bell (2003), Frequency-time spectra of magnetospherically reflecting whistlers in the plasmasphere, *J. Geophys. Res.*, *108*(A1), 1030, doi:10.1029/2002JA009387.

Bortnik, J., U. S. Inan, and T. F. Bell (2006), Temporal signatures of radiation belt electron precipitation induced by lightning-generated MR whistler waves: 1. Methodology, *J. Geophys. Res.*, *111*, A02204, doi:10.1029/2005JA011182.

Eliasson, B., and K. Papadopoulos (2008), Numerical study of mode conversion between lower hybrid and whistler waves on short-scale density striations, *J. Geophys. Res.*, *113*, A09315, doi:10.1029/2008JA013261.

Foust, F. R., U. S. Inan, T. Bell, and N. G. Lehtinen (2010), Quasi-electrostatic whistler mode wave excitation by linear scattering of EM whistler waves from magnetic field-aligned density irregularities, *J. Geophys. Res.*, *115*, A11310, doi:10.1029/2010JA015850.

Fukao, S., M. Yamamoto, R. T. Tsunoda, H. Hayakawa, and T. Mukai (1998), The SEEK (Sporadic-E Experiment over Kyushu) Campaign, *Geophys. Res. Lett.*, *25*, 1761–1764, doi:10.1029/98GL00932.

Ganguli, G., L. Rudakov, W. Scales, J. Wang, and M. Mithaiwala (2010), Three dimensional character of whistler turbulence, *Phys. Plasmas*, *17*, 052310, doi:10.1063/1.3420245.

Gemelos, E. S., U. S. Inan, M. Walt, M. Parrot, and J. A. Sauvaud (2009), Seasonal dependence of energetic electron precipitation: Evidence for a global role of lightning, *Geophys. Res. Lett.*, *36*, L21107, doi:10.1029/2009GL040396.

Helliwell, R. A. (1965), *Whistlers and Related Ionospheric Phenomena*, Stanford Univ. Press, Stanford, Calif.

Inan, U. S., and T. F. Bell (1991), Pitch angle scattering of energetic particles by oblique whistler waves, *Geophys. Res. Lett.*, *18*, 49–52, doi:10.1029/90GL02475.

Inan, U. S., T. F. Bell, J. Bortnik, and J. M. Albert (2003), Controlled precipitation of radiation belt electrons, *J. Geophys. Res.*, *108*(A5), 1186, doi:10.1029/2002JA009580.

Kagan, L. M., and M. C. Kelley (2000), A thermal mechanism for generation of small-scale irregularities in the ionospheric E region, *J. Geophys. Res.*, *105*, 5291–5303, doi:10.1029/1999JA900415.

Kelley, M. C., T. L. Arce, J. Salowey, M. Sulzer, W. T. Armstrong, M. Carter, and L. Duncan (1995), Density depletions at the 10-m scale induced by the Arecibo heater, *J. Geophys. Res.*, *100*, 17,367–17,376, doi:10.1029/95JA00063.

Lee, M. C., and S. P. Kuo (1984), Production of lower hybrid waves and field-aligned plasma density striations by whistlers, *J. Geophys. Res.*, *89*, 10,873–10,880, doi:10.1029/JA089iA12p10873.

Lehtinen, N. G., and U. S. Inan (2008), Radiation of ELF/VLF waves by harmonically varying currents into a stratified ionosphere with application to radiation by a modulated electrojet, *J. Geophys. Res.*, *113*, A06301, doi:10.1029/2007JA012911.

Lehtinen, N. G., and U. S. Inan (2009), Full-wave modeling of transionospheric propagation of VLF waves, *Geophys. Res. Lett.*, *36*, L03104, doi:10.1029/2008GL036535.

Mishin, E. V., M. J. Starks, G. P. Ginet, and R. A. Quinn (2010), Nonlinear VLF effects in the topside ionosphere, *Geophys. Res. Lett.*, *37*, L04101, doi:10.1029/2009GL042010.

Parrot, M., J. A. Sauvaud, J. J. Berthelier, and J. P. Lebreton (2007), First in-situ observations of strong ionospheric perturbations generated by a powerful VLF ground-based transmitter, *Geophys. Res. Lett.*, *34*, L11111, doi:10.1029/2007GL029368.

Pfaff, R., M. Yamamoto, P. Marionni, and S. Fukao (1998), Electric field measurements above and within a sporadic *E* layer, *Geophys. Res. Lett.*, *25*, 1769–1772, doi:10.1029/98GL00935.

Rosenberg, S., and W. Gekelman (1998), Electric field measurements of directly converted lower hybrid waves at a density striation, *Geophys. Res. Lett.*, *25*, 865–868, doi:10.1029/98GL00382.

Rosenberg, S., and W. Gekelman (2000), A laboratory investigation of lower hybrid wave interactions with a field-aligned density depletion, *Geophys. Res. Lett.*, *27*, 859–862, doi:10.1029/1999GL000005.

Rosenberg, S., and W. Gekelman (2001), A three-dimensional experimental study of lower hybrid wave interactions with field aligned density depletions, *J. Geophys. Res.*, *106*, 28,867–28,884, doi:10.1029/2000JA000061.

Schlegel, K., and C. Haldoupis (1994), Observation of the modified two-stream plasma instability in the midlatitude *E* region ionosphere, *J. Geophys. Res.*, *99*, 6219–6226, doi:10.1029/93JA02869.

Schuck, P. W., G. I. Ganguli, and P. Kintner (2002), The role of lower hybrid-wave collapse in the auroral ionosphere, *Phys. Rev. Lett.*, *89*, 065002, doi:10.1103/PhysRevLett.89.065002.

Schuck, P. W., J. W. Bonnell, and P. M. Kintner Jr. (2003), A review of lower hybrid solitary structures, *IEEE Trans. Plasma Sci.*, *31*, 1125–1177, doi:10.1109/TPS.2003.822043.

Starks, M. J., R. A. Quinn, G. P. Ginet, J. M. Albert, G. S. Sales, B. W. Reinisch, and P. Song (2008), Illumination of the plasmasphere by terrestrial very low frequency transmitters: Model validation, *J. Geophys. Res.*, *113*, A09320, doi:10.1029/2008JA013112.

Stenzel, R. L., and W. Gekelman (1975), Electrostatic waves near the lower hybrid frequency, *Phys. Rev. A*, *11*, 2057–2060, doi:10.1103/PhysRevA.11.2057.

Sudan, R. N. (1983), Unified theory of nonlinear type 1 and 2 instabilities, *J. Geophys. Res.*, *88*, 4853–4860, doi:10.1029/JA088iA06p04853.

Tsunoda, R. T., S. Fukao, M. Yamamoto, and T. Hamasaki (1998), First 24.5 MHz radar measurements of quasi-periodic backscatter from field-aligned irregularities in midlatitude sporadic *E*, *Geophys. Res. Lett.*, *25*, 1765–1768, doi:10.1029/98GL01086.

Vincena, S., W. Gekelman, M. A. Van Zeeland, J. Maggs, and A. Collette (2008), Quasielectrostatic whistler wave radiation from the hot electron emission of a laser-produced plasma, *Phys. Plasmas*, *15*, 072114, doi:10.1063/1.2956994.

Yamamoto, M., S. Fukao, R. F. Woodman, T. Ogawa, T. Tsuda, and S. Kato (1991), Midlatitude *E* region field-aligned irregularities observed with the MU radar, *J. Geophys. Res.*, *96*, 15,943–15,949, doi:10.1029/91JA01321.

Yamamoto, M., T. Itsuki, T. Kishimoto, R. T. Tsunoda, R. F. Pfaff, and S. Fukao (1998), Comparison of *E* region electric fields observed with a sounding rocket and a Doppler radar in the SEEK Campaign, *Geophys. Res. Lett.*, *25*, 1773–1776, doi:10.1029/98GL01055.

B. Eliasson, Institute for Theoretical Physics, Faculty of Physics and Astronomy, Ruhr-University Bochum, Bochum D-44780, Germany.

G. Milikh, K. Papadopoulos, X. Shao, and A. S. Sharma, Departments of Physics and Astronomy, University of Maryland, College Park, MD 20742, USA. (xshaoup@yahoo.com)